FERMI NATIONAL ACCELERATOR LABORATORY

DØ Note 6363
September 2012

# Combination of the $t\bar{t}$ production cross section measurements from the Tevatron Collider

The Tevatron Electroweak Working Group

We combine six measurements of the top-antitop ($t\bar{t}$) production cross section ($\sigma_{t\bar{t}}$) based on data collected by the CDF and D0 detectors at the Fermilab Tevatron. The datasets correspond to integrated luminosities of up to 8.8 fb$^{-1}$. We obtain a value of $\sigma_{t\bar{t}} = 7.65 \pm 0.42$ pb for a top-quark mass $m_t = 172.5$ GeV/$c^2$. The contributions to the uncertainty correspond to 0.20 pb from statistical sources, 0.29 pb from systematic sources, and 0.22 pb from from the estimated integrated luminosity. The result is in good agreement with Standard Model predictions.

## I. INTRODUCTION

The heaviest known elementary particle, and the last missing member of the three families of quarks, the top quark, was discovered in 1995 [1, 2] by the CDF and D0 experiments at the Tevatron proton-antiproton ($p\bar{p}$) collider. Its high mass and its short lifetime make the top quark especially interesting. The short lifetime of the top quark of about $10^{-25}$s [3, 4], which is far shorter than the timescale for hadronization, provides the opportunity to study what is essentially a free quark. Its high mass suggests that the top quark may play a special role in the mechanism of electroweak symmetry breaking, and thereby provides a window on physics beyond the Standard Model (SM).

The first natural step in understanding the top quark is through a precise determination of its production mechanisms and their rates, and in comparing them to SM predictions. Various models for physics beyond the SM (BSM) predict effects in the top sector that can change the observed production cross section, as, for example from the decay of the top quark into a charged Higgs boson and a $b$ quark [5].

### A. Predictions for the $t\bar{t}$ cross section

Production of top quarks at hadron colliders takes place through strong interactions that yield $t\bar{t}$ pairs, or through electroweak processes that produce single top quarks. At the Tevatron $p\bar{p}$ collider, with a center of mass energy of $\sqrt{s} = 1.96$ TeV, the dominant production process is $t\bar{t}$ production. At next-to-leading-order (NLO) in quantum chromodynamics (QCD), contributions to $t\bar{t}$ production are $\approx 85\%$ from quark-antiquark annihilation ($q\bar{q} \to t\bar{t}$) and $\approx 15\%$ from gluon-gluon fusion ($gg \to t\bar{t}$).

SM predictions for the inclusive $t\bar{t}$ cross section at the Tevatron calculated to different orders in perturbative QCD are available in the literature. The first calculation in full NLO QCD was performed before the discovery of the top quark [6], and has been updated to use recent CTEQ6.6 parton distributions functions (PDF) [7]. Furthermore, several results with the complete NLO calculation have been improved by adding reesummations of higher order logarithmic corrections to the cross section due to soft-gluon radiation. In particular, the inclusion of next-to-leading logarithmic (NLL) soft-gluon resummations [8] using modern sets of PDF are available [9]. Several NLO QCD calculations with inclusion of soft-gluon resummations to next-to-next-to-leading logarithmic (NNLL) accuracy also exist, as well as calculations that approximate the next-to-next-to-leading-order (NNLO) QCD, derived from NLO+NNLL results by re-expanding the latter in a fixed-order series in $\alpha_s$ ($\text{NNLO}_{\text{approx}}$) [10–13]. The calculations performed to NLO+NNLL and $\text{NNLO}_{\text{approx}}$ level of QCD differ in the way the threshold resummations are implemented. For example, whether the resummation uses a momentum-space approach or N-space resummation, whether the total cross section is resummed, or whether a differential cross section is used, that which is integrated over phase space after resummation. Details of these specifics can be found in Ref. [10–13].

To estimate the uncertainty on predicted cross sections, the factorization and renormalization scales are changed by factors of two relative to the central values for a given top-quark mass ($m_t$). The sensitivity of the measured cross sections to the choice of PDF are evaluated by varying standard parameter sets used to determine the effects of their uncertainties [7].

For some of the approximate NNLO calculations performed through differential cross section additional uncertainties are added, for example, from the choice of the differential distribution which is then subsequently integrated to obtain the total cross section. A summary of differences in the calculations can be found in Ref. [13]. While most SM predictions for $\sigma_{t\bar{t}}$ are calculated using the pole mass of the top quark as input, it is known that the pole mass cannot be defined unambiguously in QCD. Recent calculations use the top-quark mass as defined in the $\overline{MS}$ scheme [10, 11]. Also new results at full fixed-order NNLO QCD, as well as at NNLO+NNLL QCD have recently been published for $q\bar{q} \to t\bar{t}$. The second calculation reduces the uncertainty on $\sigma_{t\bar{t}}$ to $\approx 2.7\%$ [14]. An overview of the predictions at different orders in QCD is given in Table 1.

TABLE 1: An overview of SM predictions of $\sigma_{t\bar{t}}$ at different orders in perturbative QCD, using the program described in Ref. [15]. The top-quark mass for these calculations is set to $m_t = 172.5$ GeV/$c^2$ and use the MSTW2008nlo68cl or MSTW2008nnlo68cl PDF [16].

| Calculation | $\sigma_{t\bar{t}}$ (pb) | $\Delta\sigma_{\text{scale}}$ (pb) | $\Delta\sigma_{\text{PDF}}$ (pb) |
|---|---|---|---|
| NLO | 6.85 | $^{+0.37}_{-0.77}$ | $^{+0.19}_{-0.13}$ |
| NLO+NLL | 7.09 | $^{+0.28}_{-0.51}$ | $^{+0.19}_{-0.13}$ |
| NNLO+NNLL | 7.24 | $^{+0.15}_{-0.24}$ | $^{+0.18}_{-0.12}$ |

### B. Channels for the combination

Within the SM, the top quark decays via the weak interaction into a $W$ boson and a down-type quark. The decay $t \to W^+b$, and its charge conjugate, occur with almost 100% probability. The $W$ boson subsequently decays either leptonically into $e\bar{\nu}_e$, $\mu\bar{\nu}_\mu$ or $\tau\bar{\nu}_\tau$, or into $u\bar{d}$ or $c\bar{s}$ quarks. In studies of $t\bar{t}$ events, different channels are defined according to the decays of the two $W$ bosons. The main channels are:

- **All-jets:** With a probability of about 46%, the all-jets channel, where both $W$ bosons decay hadronically, is the dominant $t\bar{t}$ final state. Experimentally, this channel suffers from a large background from multijet production.

- **Lepton+jets:** This final state ($\ell$+jets) consists of events where one $W$ boson decays hadronically and the other into $e\bar{\nu}_e$, $\mu\bar{\nu}_\mu$, or $\tau\bar{\nu}_\tau$, where the $\tau$ decays leptonically. The branching fraction of this channel is approximately 35%. The main background contribution in this channel arises from $W$+jets production.

- **Dilepton:** Events where both $W$ bosons decay into $e\bar{\nu}_e$, $\mu\bar{\nu}_\mu$, or $\tau\bar{\nu}_\tau$ where the $\tau$ decays leptonically, comprise the dilepton final state. While the branching fraction for this channel is only about 4%, it is a very clean final state, with very contribution from background.

The final states where one of the $W$ bosons decays into $\tau\bar{\nu}_\tau$ and the $\tau$ decays into hadrons comprise separate channels, namely the $\tau$+lepton and $\tau$+jets final states. These two final states are challenging due to the more difficult reconstruction of the hadronic decay mode of the $\tau$ and these measurements are not used in this combination.

In this paper, we combine results of $\sigma_{t\bar{t}}$ in the all-jets, the $\ell$+jets and the dilepton final states studied by the CDF and D0 collaborations.

### C. Selection and modeling

The $t\bar{t}$ cross section measurement in each individual final state requires specific event-selection criteria to enrich the $t\bar{t}$ content of each sample, a detailed understanding of background contributions, as well as of the modeling of the signal and all the individual background processes. In this section, these essentials are briefly discussed. The CDF and D0 detectors are described in Refs. [17] and [18], respectively.

#### *1. Event selection*

Candidate $t\bar{t}$ events are first collected through high-pT lepton, lepton+jets or multijet triggers depending on the channels. The selection of enriched $t\bar{t}$ samples relies then on the differences in topology and kinematics of the $t\bar{t}$ events and the background contributions in any final state. The basic objects we use at CDF and D0 for these selections are jets, electrons, muons, and imbalance in transverse momentum ($\not\!\!p_T$). At D0, jets are reconstructed using a cone algorithm [19] of $\mathcal{R} = 0.5$ [20], while CDF implements an algorithm [21] with $\mathcal{R} = 0.4$. Electrons are reconstructed using mainly information from the electromagnetic calorimeter, but also require a track that is matched to the calorimeter cluster. Muons are reconstructured using information from the outer muon system, and also a matching track in the central tracking system. For both electrons and muons, isolation criteria are applied to identify the charged leptons from the $W \to \ell\bar{\nu}_\ell$ decay. The primary interaction vertex is required to be reconstructed within 60 cm of the longitudinal center of the detector. A common feature of $t\bar{t}$ events in all the final states are the two $b$-jets from the $t \to Wb$ decays. The identification and requirement of $b$-jets in these events therefore helps to enrich the sample in $t\bar{t}$ content. At D0, a neural-net (NN) based $b$-jet identification algorithm is used for this purpose [22], while at CDF $b$-jets are identified based on information from a displaced, secondary vertex [23]. The NN based $b$-tagging algorithm at D0 combines into a single discriminant information about the impact parameters of the tracks and the properties of the reconstructed secondary vertices.

The imbalance in transverse momentum $\not\!\!p_T$ is reconstructed using the energy deposited in calorimeter cells, incorporating corrections for the transverse momentum ($p_T$) of leptons and jets. More details on identification criteria at CDF and D0 can be found in Ref. [24].

The all-jets final state requires at least six jets with large $p_T$ located at central pseudorapidities ($\eta$) [20]. Events containing an isolated electron or muon are vetoed, and the $\not\!\!p_T$ has to be small. In the $\ell$+jets channel, selected events must have at least three high-$p_T$ jets, one high-$p_T$ isolated electron or muon within some chosen fiducial region, and a large $\not\!\!p_T$ to account for the escaping neutrino from the $W \to \ell\bar{\nu}_\ell$ decay. In addition, requirements on the number of identified $b$-jets are applied to reduce background, and requirements on the azimuthal angle between the lepton direction and $\not\!\!p_T$ are applied to reduce contributions from multijet background. Dilepton $t\bar{t}$ events are selected by requiring at least two jets with high $p_T$ and central $\eta$, two high-$p_T$ isolated leptons of opposite charge, and large $\not\!\!p_T$. Additional selections based on the global properties of the event are applied to the $e^+e^-$, $e^\pm\mu^\mp$ or $\mu^+\mu^-$ final states.

#### *2. Signal modeling*

Independent of the final state, a proper modeling of the signal and background processes is crucial for assessing the event selections and the calibration of the extracted $\sigma_{t\bar{t}}$. At D0, $t\bar{t}$ production and decay are simulated using the ALPGEN Monte Carlo (MC) program [25]. Parton showering and hadronization are simulated using PYTHIA [26]. Double-counting of partonic event configurations is avoided using a matching scheme [27]. The MC-generated events are then processed through a GEANT-based [28] simulation of the D0 detector. Additional $p\bar{p}$ interactions are modeled by overlaying data from random $p\bar{p}$ crossings on the MC events. Finally, the events are reconstructed with the same algorithms used for data events. At CDF, $t\bar{t}$ events are simulated using PYTHIA, and afterwards processed through

CDFSIM, a GEANT-based simulation of the CDF detector [29, 30]. In both collaborations, additional correction factors are implemented to take into account differences between data and MC. In particular, these are corrections made to the jet energy scale (JES), jet energy resolution (JER), electron and muon energy scale, trigger efficiencies, and $b$-jet identification. Details about these corrections can be found in Refs. [31–35]. The central top quark mass used for the measurements of the cross section is $m_t = 172.5$ GeV. At D0, the CTEQ6L1 PDF are used for MC event generation [36], while CDF uses the CTEQ6.6 [7] or CTEQ5L PDF [37].

#### *3. Background modeling*

Different sources of background contribute to the different final states. In the dilepton channel, the dominant source of background arises from $Z/\gamma^*$+jets production, with the $Z/\gamma^*$ decaying into a lepton pair. In addition, diboson production ($WW$, $WZ$, and $ZZ$) and instrumental background arising from multijet and $W$+jets production, where a jet is misidentified as a lepton, contribute to the dilepton final state. At CDF, $W\gamma$ production is also considered separately, while at D0 this contribution is accounted for as part of the instrumental background when the $\gamma$ is misidentified as a lepton or a jet. For $\ell$+jets final states, the major background contribution is from $W$+jets production, when the $W$ boson decays into $\ell\bar{\nu}_\ell$. Furthermore, backgrounds from single top-quark production, diboson production, $Z$+jets and multijet production are considered. The dominant background contribution to all-jets events is from multijet production.

The contributions from $Z/\gamma^*$+jets and $W$+jets backgrounds are modeled using ALPGEN, followed by PYTHIA for parton showering and hadronization. Contributions from heavy flavor (HF) quarks, namely from $W + b\bar{b}$, $W + c\bar{c}$, $Z/\gamma^* + b\bar{b}$, $Z/\gamma^* + c\bar{c}$ are simulated separately.

The diboson contributions in the dilepton and $\ell$+jets final states are simulated using PYTHIA, normalized to the NLO cross section calculated using MCFM [38]. Single top-quark contributions are simulated using the COMPHEP generator [39] at D0, and MADEVENT [40] at CDF, and normalized to the approximate NNNLO [41] or the NLO [42] prediction, respectively. The separated background contribution from $W\gamma$ production at CDF is simulated using the BAUR MC [43].

The instrumental and multijet backgrounds are estimated using data-driven methods in different ways for the different final states both at CDF and D0.

## II. INPUTS TO THE COMBINATION

CDF and D0 have performed many measurements of the $t\bar{t}$ production cross section. In this paper, we present a combination based on six of these measurements with the goal of reducing the experimental uncertainty and thereby improving the test of the theoretical prediction. We first combine four CDF measurements to obtain the best CDF estimate. Then, we combine this CDF result with a previously published combination of two D0 measurements to obtain the Tevatron's best estimate of the inclusive $t\bar{t}$ cross section.

### A. CDF measurements and their combination

CDF includes the following four measurements in the combination: one from the dilepton channel (DIL) [31], one from the all-jets channel (HAD) [32] and two from the lepton+jets channel [33].

The measurement in the dilepton channel using 8.8 fb$^{-1}$ of data relies on counting events with at least one identified $b$-jet. Backgrounds from diboson and $Z/\gamma^*$ events are predicted from simulation, corrected to reproduce the data. The largest uncertainties for this measurement come from the uncertainty on the measured luminosity and on the modeling of $b$ tagging.

The two measurements in the $\ell$+jets channel, performed by CDF using 4.6 fb$^{-1}$ of data, exploit complementary methods to discriminate signal from background. The first one exploits differences in kinematic properties of signal and $W$+jets background without using $b$ tagging, and is referred to as LJ-ANN in the following. Because of the large mass of the top quark, remnants of $t\bar{t}$ have larger $p_T$, and are more central and isotropic relative to the main backgrounds from $W$+jets and multijet production. Seven kinematic variables are selected for input to an artificial neural network. Since $W$+jets production is the dominant background in the data before implementation of $b$ tagging, the neural network is trained using only $t\bar{t}$ and $W$+jets MC samples. The number of $t\bar{t}$ events is extracted from a fit of the neural network output distribution in the $W+ > 2$ jets data. The largest systematic uncertainties come from the calibration of jet energy and modeling of the $t\bar{t}$ signal.

The second $\ell$+jets measurement reconstructs displaced secondary vertices to identify $b$-jets and thereby suppresses the dominant $W$+jets background. In the following this analysis is referred to as LJ-SVX. The number of events with at least one $b$-tagged jet is studied in data and simulation, and since the relative fraction of HF production in the simulated $W$+jets ALPGEN events is found to be underestimated, a correction factor obtained from data is applied to produce agreement. The number of $W$+HF events in the $b$-tagged sample is estimated by applying this correction factor and a tagging efficiency to the predicted number of $W$+HF events prior to $b$ tagging (pretag). The fraction of mistagged events in the $b$-tagged data is found by applying the parameterized mistag probability function to the pretagged data. The $t\bar{t}$ cross section is then extracted from a likelihood fit to the number of tagged events in data, given the predicted background. The largest systematic uncertainties in this method arise from the correction factor for the $W$+HF background, the modeling of $b$ tagging in the MC simulation, and the measured integrated luminosity.

To reduce the large uncertainty on the luminosity both CDF $\ell$+jets measurements exploit the correlation in luminosity between $Z$ boson and $t\bar{t}$ production, through the ratio of the $t\bar{t}$ to the $Z$ boson cross section, measured using the same triggers and data. This is multiplied by the precisely known theoretical $Z$ cross section [44], replacing thereby the uncertainty on luminosity with the smaller theoretical and experimental uncertainties on the $Z$ cross section.

In the all-jets final state, the signal sample is selected by requiring from six to eight jets in the event. Further selection is applied by requiring the presence of $b$-tagged jets and by cutting on the value of a neural network discriminator (NN). This NN makes use of 13 observables and is trained to suppress the large backgrounds from multijet events. To improve the statistical significance of the measurement, the cut on the NN value is optimised seperately for events with only one $b$-tagged jet and for those with more than one. Using 2.9 fb$^{-1}$ of data, the cross section is extracted from a fit to the reconstructed top quark mass for events with one and with more than one $b$-jet. The largest uncertainties arise from the calibration of jet energy, the normalization of the background estimated from data, and the luminosity.

To combine the CDF measurements, a best linear unbiased estimate (BLUE) [45–47] is formed for the $t\bar{t}$ production cross section. This is done by constructing a covariance matrix from the statistical and systematic uncertainties of each result, taking into account the statistical and systematic correlations. This covariance matrix is inverted to obtain a weight for each result, and to combine the results using these weights to obtain the best estimate. The technique is designed to provide the best total uncertainty on the combined result. It is checked with simulated experiments and found to be unbiased.

The two results in the CDF $\ell$+jets channel use subsets of events that pass common $\ell$+jets selections. Their statistical correlation is evaluated through 1,000 simulated experiments. The $t\bar{t}$ cross section is extracted for each such pseudo-experiment, for LJ-ANN, through a maximum likelihood fit to the neural network distribution, and for LJ-SVX, through the observed number of $b$-tagged events in each pseudo-experiment. The statistical correlation between two measurements is determined to be 32%. To study the stability of the combined cross section with respect to systematic shifts in their statistical correlation, the latter value was varied by $\pm 10\%$, resulting in a change in uncertainty of $< 0.01$ pb.

Table 2 summarizes the four CDF inputs to the combination with their uncertainties, as well as their combined result for $m_t = 172.5$ GeV, which yields

$$\sigma_{t\bar{t}}(\text{CDF}) = 7.71 \pm 0.31\,(\text{stat}) \pm 0.37\,(\text{syst}) \pm 0.15\,(\text{lumi})\ \text{pb}.$$

Detailed description of sources of uncertainties and their correlations are given in Section III.

| | DIL | LJ-ANN | LJ-SVX | HAD | CDF combined |
|---|---|---|---|---|---|
| Central value of $\sigma_{\bar{t}t}$ | 7.47 | 7.82 | 7.32 | 7.21 | 7.71 |
| Uncertainties | | | | | |
| Statistical | 0.50 | 0.38 | 0.36 | 0.50 | 0.31 |
| Detector modeling | 0.41 | 0.11 | 0.34 | 0.41 | 0.17 |
| Signal modeling | 0.24 | 0.23 | 0.23 | 0.44 | 0.22 |
| Jet modeling | 0.25 | 0.23 | 0.29 | 0.71 | 0.21 |
| Method | 0.00 | 0.01 | 0.01 | 0.08 | 0.01 |
| Background from theory | 0.02 | 0.13 | 0.29 | 0.00 | 0.10 |
| Background based on data | 0.10 | 0.07 | 0.11 | 0.59 | 0.07 |
| $Z$ boson theoretical normalization | 0.00 | 0.16 | 0.15 | 0.00 | 0.13 |
| Inelastic $p\bar{p}$ cross section | 0.31 | 0.00 | 0.00 | 0.30 | 0.05 |
| Luminosity detector | 0.30 | 0.02 | 0.02 | 0.29 | 0.06 |
| Total systematics | 0.70 | 0.41 | 0.61 | 1.18 | 0.40 |

TABLE 2: CDF measurements of $\sigma_{\bar{t}t}$ and their combination, with breakdown shown for uncertainties (in pb).

The total uncertainty of the CDF combined cross section is 0.50 pb. The measurement in the $\ell$+jets channel using the LJ-ANN carries the largest weight of 70%, followed by the dilepton result with 22%, while the measurement using $b$-jet identification in the $\ell$+jets channel has a weight of 15%. The measurement in the all-jets channel has a weight of $-7\%$. This situation can occur if the correlation between two measurements is larger than the ratio of

their total uncertainties [45]. The correlation matrix, including statistical and systematic effects, is given in Table 3. The largest correlations are 51% between the LJ-ANN and LJ-SVX measurements, from the overlap in events, and the correlation in systematics between the acceptance and luminosity; and a correlation of 52% between the DIL and HAD measurements, due to the correlation in systematics for the acceptance, $b$ tagging and luminosity.

| Correlation | LJ-ANN | LJ-SVX | DIL | HAD |
|---|---|---|---|---|
| LJ-ANN | 1 | 0.51 | 0.26 | 0.34 |
| LJ-SVX | | 1 | 0.45 | 0.48 |
| DIL | | | 1 | 0.52 |
| HAD | | | | 1 |

TABLE 3: CDF total correlation matrix, including statistical and systematic correlations.

### B. D0 measurements and their combination

D0 includes two measurements in the combination: one from the dilepton channel [34] and one from the lepton+jets channel [35].

In the $\ell$+jets channel, D0 performed a $t\bar{t}$ cross section measurement with 5.3 fb$^{-1}$ of data by selecting events with greater than one jet, and splitting these into subsamples according to the number of jets and $b$-jets. In the background-dominated subsamples, i.e., two-jet events, three-jet events with less than two $b$-jets, and events with at least four jets and no $b$-jets, a mulitvariate discriminant called Random Forest (RF) is used to separate signal from background. In samples with large signal fraction, i.e. events with at least four jets or three jets with two $b$-jets, the event yields are used. The cross section is then extracted by simultaneously fitting the RF discriminant in the background dominated samples and performing a counting method in the signal dominated channels. use a $b$ tagging counting method to extract the cross section through a simultaneous fit This is done for distributions with different jet multiplicities, and by constraining many systematic uncertainties through Gaussian constrained "nuisance" parameters that are minimized in the fit to data. The dominant systematic uncertainty of this measurement is from the determination of the integrated luminosity.

In the dilepton channel, using 5.4 fb$^{-1}$ of data, D0 measures $\sigma_{t\bar{t}}$ from a likelihood fit to the discriminant based on the NN-based $b$-tagging algorithm. The cross section is extracted from a fit to the distribution of the smallest of the two $b$-tagging NN output values of the two jets with highest energy. The result is dominated by the uncertainty on the integrated luminosity.

The measurements in the dilepton and $\ell$+jets channels are combined using the same "nuisance" parameter technique used in the individual measurements, taking into account the correlations among common systematic uncertainties. The result of the combination of the D0 results yields [35]

$$\sigma_{t\bar{t}}(\mathrm{D0}) = 7.56^{+0.63}_{-0.56}\,(\mathrm{stat}+\mathrm{syst})\ \mathrm{pb}.$$

for a top-quark mass of 172.5 GeV. For the combination presented in this paper, the uncertainties of the D0 result have been symmetrized and the statistical and systematic uncertainties have been split.

## III. OVERVIEW OF SYSTEMATIC UNCERTAINTIES

In combining the results, the uncertainties are divided into 10 categories that provide a straightforward way to account for their correlations. Most categories involve more than one source of uncertainty, but have identical correlations pattern to facilitate their combination. We discuss below each component used in the combined cross section. The values of the CDF and D0 systematic uncertainties are summarized in Table 4.

### A. Detector modeling

For both experiments this category includes uncertainties on the trigger and lepton-identification efficiency, on the $b$ tagging efficiency and on the modeling of multiple $p\bar{p}$ interactions. In addition, for CDF measurements, this category includes the uncertainty on the fraction of the luminous region within the acceptance of the CDF detector. Also included are the track identification efficiencies for LJ-ANN and LJ-SVX measurements and the uncertainty on

| | CDF | D0 | | Tevatron |
|---|---|---|---|---|
| Central value of $\sigma_{\bar{t}t}$ | 7.71 | 7.56 | | 7.65 |
| Uncertainties | | | Corr. | |
| Statistical | 0.31 | 0.20 | no | 0.20 |
| Detector modeling | 0.17 | 0.22 | no | 0.13 |
| Signal modeling | 0.22 | 0.13 | yes | 0.18 |
| Jet modeling | 0.21 | 0.11 | no | 0.13 |
| Method | 0.01 | 0.07 | no | 0.03 |
| Background from theory | 0.10 | 0.08 | yes | 0.10 |
| Background based on data | 0.07 | 0.06 | no | 0.05 |
| $Z$ boson theoretical normalization | 0.13 | 0.00 | yes | 0.08 |
| Inelastic $p\bar{p}$ cross section | 0.05 | 0.32 | yes | 0.16 |
| Luminosity detector | 0.06 | 0.33 | no | 0.14 |
| Total systematic | 0.40 | 0.56 | | 0.36 |

TABLE 4: Input cross sections from each experiment, breakdown of their uncertainties (in pb), and the result of the Tevatron combination. The column "Corr." indicates if a given uncertainty is treated as 100% correlated between the CDF and D0 measurements in the combination.

the lepton-energy scale. For D0 measurements, additional uncertainties entering into this category arise from vertex reconstruction and identification efficiency and lepton-energy resolution. Since all sources of uncertainties are specific to the CDF and D0 detectors, they are treated as uncorrelated in combining the results.

### B. Signal modeling

The uncertainties in this category arise from several sources, and are taken to be fully correlated among the CDF and D0 measurements.

- **$t\bar{t}$ MC generator**: For both CDF and D0 measurements this uncertainty includes the difference between PYTHIA and HERWIG [48] resulting from different models for hadronization and for the underlying event. D0 measurements also evaluate uncertainties due to higher-order QCD corrections to the matrix element describing $t\bar{t}$ production by comparing ALPGEN to MC@NLO [49].

- **Parton distribution functions**: The uncertainties on the PDF eflect the uncertainty on determining the probability of finding a particular parton carrying a particular fraction of the proton's momentum. This in turn affects the kinematics of the final-state particles in $t\bar{t}$ production and decay, as well as the selection efficiency, and the distributions in the final state. The default acceptance is calculated using the leading-order CTEQ5L (CTEQ6L) for CDF (D0). The systematic uncertainty includes the uncertainties evaluated using NLO error vectors from CTEQ6M (CDF) and CTEQ6.1M (D0) following the prescription of the CTEQ collaboration [50]. CDF also includes the difference between the central value for leading-order and next-to-leading order PDF in this systematic uncertainty.

- **Initial and final-state radiation**: The amount of QCD radiation from partons in the initial (ISR) or final (FSR) state is set by parameters of the PYTHIA generator used to simulate $t\bar{t}$ events. The uncertainties of these parameters are taken from a study of ISR in Drell-Yan events: $q\bar{q} \to Z/\gamma^* \to \mu\mu$, that share the same initial $q\bar{q}$ state as most of the $t\bar{t}$ signal [51].

- **Color reconnection**: This uncertainty is evaluated by comparing PYTHIA tunes with different parameters that affect the exchange of momentum and energy via gluons between the top-quark decay chain and the color-connected anti top-quark decay chain. In particular, the difference between the $t\bar{t}$ efficiency obtained with PYTHIA using the A-PRO and the ACR-PRO tunes is quoted as the systematic uncertainty.

- **Decay branching fractions for $W$ bosons**: This uncertainty affects the $t\bar{t}$ acceptance, and is evaluated by changing the branching fractions in the $W$-boson decay by their uncertainties [52].

### C. Jet modeling

Uncertainties on modeling jets affect the $t\bar{t}$ acceptance and kinematic distributions used to extract the cross section. They arise from the calibration of light-quark and $b$-jet energies, and the modeling of jet reconstruction and resolution in the MC simulation. Since jet-modeling uncertainties are dominated by detector-specific effects, they are treated as uncorrelated between results from CDF and D0.

- **Jet energy scale**: This uncertainty arises from the uncertainties of calibration of the jet energy which is performed using test-beam data (CDF), as well as $\gamma$+jets and dijet events at CDF and D0. The effect on the measurement is evaluated by replacing the $t\bar{t}$ MC sample used in the measurements by one with jet energies changed by their estimated systematic uncertainties.
- ***b*-jet energy scale**: This uncertainty considers the difference in jet energy scale between jets from light quarks or gluons, and from $b$ quarks. For CDF, it includes the three sources: (i) uncertainties on branching fractions of semileptonic decays of $b$ and $c$ quarks; (ii) uncertainties on $b$-quark fragmentation parameters, (iii) uncertainty on the calorimeter response to $b$ and $c$ hadrons. For D0, the sources are uncertainties on fragmentation parameters of the $b$-quark in the $t\bar{t}$ simulation, and the difference in calorimeter response to jets from $b$ and light quarks.
- **jet reconstruction and identification**: This uncertainty is specific to D0, and covers the uncertainty on the correction factors applied to simulation to match jet identification efficiency in data, and on the factors used to adjust jet resolution in simulation to that observed in data.

### D. Method of extraction of $\sigma_{t\bar{t}}$

This uncertainty is unique to a particular method, and arises from limited MC statistics, from limitations in statistics in forming the MC templates or from the dependence of the calibration on the specific analysis. It is uncorrelated among different measurements.

### E. Background from theory

This uncertainty for both experiments includes sources such as the uncertainty on the heavy-flavor fraction of the $W$+jets background, uncertainties on the normalization of the electroweak background, and a variation of the renormalization and factorization scale in the $W$+jets MC simulation. Since these uncertainties are related to the theoretical description of the background, this source is treated as correlated between all measurements.

### F. Background based on data

This source covers the uncertainties on the multijet background in both experiments, as well as on the uncertainty on the modeling of $Z/\gamma^*$+jets background obtained using data for D0, and the uncertainties on the mistagging of jets from charm and light-flavor quarks as $b$-jets at CDF. This source is considered uncorrelated between all measurements.

### G. *Z* boson theoretical normalization

This uncertainty is applicable only to the LJ-ANN and LJ-SVX measurements by CDF that exploit the ratio of the observed $t\bar{t}$ production rate, to the observed $Z$ boson production rate normalized by the theoretical prediction for $Z$ boson production [53]. It includes two components: (i) the variation of the renormalization and factorization scale for $Z/\gamma^*$+jets simulation, and on the background in the $Z/\gamma^*$+jets measured cross section, (ii) the uncertainty on the theoretical calculation of the $Z/\gamma^*$+jets cross section which contributes to the systematic uncertainties.

### H. Inelastic $p\bar{p}$ cross section

This source reflects the uncertainty on the CDF and D0 determination of luminosity, estimated as 4% on the total inelastic $p\bar{p}$ cross section [54], which is fully correlated among all the measurements. This source is not applicable to CDF LJ-ANN and LJ-SVX measurements that exploit the ratio to the Z boson production rate.

### I. Luminosity detector

This corresponds to the rest of the uncertainty on the luminosity that arises from detector effects [55] which is around 4.5%, and is taken to be uncorrelated between CDF and D0 measurements. This source barely affects the CDF LJ-ANN and LJ-SVX measurements that exploit the ratio to the Z boson production rate.

## IV. RESULTS

The combination of CDF and D0 $t\bar{t}$ cross sections is performed using the BLUE method as described in Section II, with inputs from the first two columns of Table 4. The result of the combination is

$$\sigma_{t\bar{t}}(\text{Tev}) = 7.65 \pm 0.20\,(\text{stat}) \pm 0.29\,(\text{syst}) \pm 0.22\,(\text{lumi})\ \text{pb}.$$

with the breakdown of systematic uncertainties given in the last column of Table 4. Adding the separate uncertainties in quadrature, the total uncertainty is 0.42 pb. The combined CDF input carries a weight of 60%, while the D0 measurement has a weight of 40%. The correlation between the two inputs is 18%. Figure 1 shows the summary of the input $t\bar{t}$ cross section measurements that enter the combination, as well as the result of this combination.

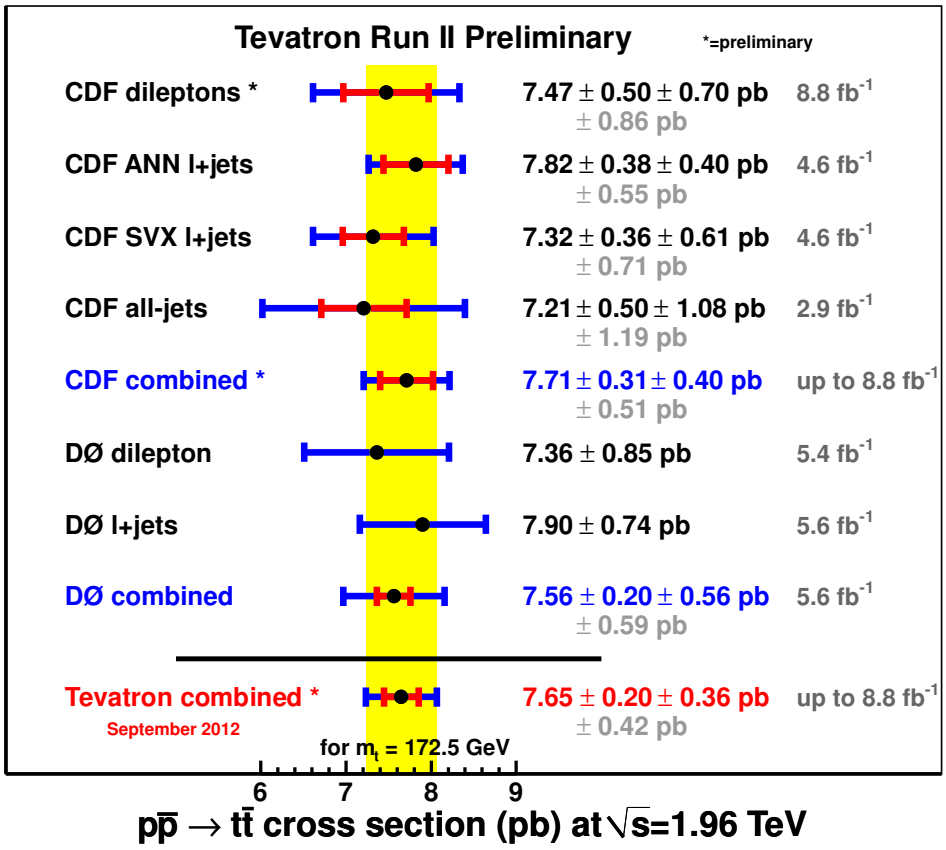


FIG. 1: (color online). The six input measurements of inclusive $\sigma_{t\bar{t}}$ from the CDF and D0 experiments, along with the separately combined CDF and D0 measurements, and the all-combined Tevatron result. The uncertainty on the D0 dilepton and $\ell$+jets measurements that use "nuisance" parameters are presented as published with only their total uncertainties. The red bars show the statistical uncertainty while the blue ones show the total uncertainties on each measurement.

## V. CONCLUSION

We have presented the combination of the $t\bar{t}$ production cross section in the $\ell$+jets, dilepton and all-jets final state using data collected by the CDF and D0 collaborations, using between 2.1 fb$^{-1}$ and 8.8 fb$^{-1}$ of data from the Tevatron $p\bar{p}$ collider. We obtain

$$\sigma_{t\bar{t}} = 7.65 \pm 0.42 \text{ pb}$$

for a top-quark mass of 172.5 GeV. The combined $\sigma_{t\bar{t}}$ measurement has a relative uncertainty of 5.5%, dominated by the systematic uncertainty from the luminosity and from signal modeling. Our result is consistent with the latest theoretical prediction of $\sigma_{t\bar{t}} = 7.24^{+0.24}_{-0.27}$ pb [14], calculated at NNLO+NNLL in perturbative QCD.

### Acknowledgments

We thank the Fermilab staff and the technical staffs of the participating institutions for their vital contributions. This work was supported by the U.S. Department of Energy and National Science Foundation. We thank the CDF collaboration institutions: the Italian Istituto Nazionale di Fisica Nucleare; the Ministry of Education, Culture, Sports, Science and Technology of Japan; the Natural Sciences and Engineering Research Council of Canada; the National Science Council of the Republic of China; the Swiss National Science Foundation; the A.P. Sloan Foundation; the Bundesministerium für Bildung und Forschung, Germany; the Korean World Class University Program, the National Research Foundation of Korea; the Science and Technology Facilities Council and the Royal Society, UK; the Russian Foundation for Basic Research; the Ministerio de Ciencia e Innovación, and Programa Consolider-Ingenio 2010, Spain; the Slovak R&D Agency; the Academy of Finland; and the Australian Research Council (ARC); and the D0 collaboration institutions: CEA and CNRS/IN2P3 (France); MON, NRC KI and RFBR (Russia); CNPq, FAPERJ, FAPESP and FUNDUNESP (Brazil); DAE and DST (India); Colciencias (Colombia); CONACyT (Mexico); NRF (Korea); FOM (The Netherlands); STFC and the Royal Society (United Kingdom); MSMT and GACR (Czech Republic); BMBF and DFG (Germany); SFI (Ireland); The Swedish Research Council (Sweden); and CAS and CNSF (China).

[1] F. Abe *et al.* (CDF Collaboration), Phys. Rev. Lett. **74**, 2626 (1995).
[2] S. Abachi *et al.* (D0 Collaboration), Phys. Rev. Lett. **74**, 2632 (1995).
[3] T. Aaltonen *et al.* (CDF Collaboration), Phys. Rev. Lett. **102**, 042001 (2009); **105**, 232003 (2010); V.M. Abazov *et al.* (D0 Collaboration), Phys. Rev. Lett. **106**, 022001 (2011); Phys. Rev. D **85**, 091104 (2012).
[4] M. Jeżabek and J.H. Kühn, Phys. Rev. D **48**, 191 (1993).
[5] V. M. Abazov *et al.*, Phys. Lett. B **682**, 278 (2009); V. M. Abazov *et al.*, Phys. Rev. D **80**, 071102 (2009); V. M. Abazov *et al.*, Phys. Rev. D **80**, 051107 (2009).
[6] P. Nason, S. Dawson and R. K. Ellis, Nucl. Phys. B **303**, 607 (1988); W. Beenakker *et al.*, Phys. Rev. D 40, 54 (1989).
[7] P. M. Nadolsky *et al.*, Phys. Rev. D **78**, 013004 (2008).
[8] R. Bonciani *et al.*, Nucl. Phys. B **529**, 424 (1998) [Erratum-ibid. B 803, 234 (2008)].
[9] M. Cacciari *et al.*, J. High Energy Phys. **0404**, 068 (2004).
[10] V. Ahrens, A. Ferroglia, M. Neubert, B. D. Pecjak, and L. L. Yang, J. High Energy Phys. **09**, 097 (2010); V. Ahrens, A. Ferroglia, M. Neubert, B. D. Pecjak, and L. L. Yang, Nucl. Phys. Proc. Suppl. **205-206**, 48 (2010); V. Ahrens, A. Ferroglia, M. Neubert, B. D. Pecjak, and L. L. Yang, Phys.Lett.B **703**, 135 (2011).
[11] S. Moch and P. Uwer, Phys. Rev. D **78**, 034003 (2008); U. Langenfeld, S. Moch, and P. Uwer, Phys. Rev. D **80**, 054009 (2009); S. Moch, P Uwer and A. Vogt, arXiv:1203.6282.
[12] N. Kidonakis and R. Vogt, Phys. Rev. D **68**, 114014 (2003); N. Kidonakis, Phys. Rev. D **82**, 114030 (2010); N. Kidonakis, arXiv:1109.3231.
[13] M. Cacciari, M. Czakon, M. L. Mangano, A. Mitov and P. Nason, Phys. Lett. B **710**, 612 (2012).
[14] P. Baernreuther, M. Czakon and A. Mitov, arXiv:1204.5201v1 (2012).
[15] M. Czakon and A. Mitov, arXiv:1112.5675.
[16] A. D. Martin, W. J. Stirling, R. S. Thorne and G. Watt, Eur. Phys. J. C **63**, 189 (2009).
[17] D.E. Acosta *et al.* (CDF Collaboration), Phys. Rev. D **71**, 052003 (2005).
[18] S. Abachi *et al.* (D0 Collaboration), Nucl. Instrum. Methods in Phys. Res. Sect. A **338**, 185 (1994); V.M. Abazov *et al.* (D0 Collaboration), Nucl. Instrum. Methods in Phys. Res. Sect. A **565**, 463 (2006); V.M. Abazov *et al.*, Nucl. Instrum. Methods in Phys. Res. Sect. A **552**, 372 (2005).
[19] G.C. Blazey *et al.*, Proceedings of the Workshop on QCD and Weak Boson Physics in Run II, edited by U. Baur, R.K. Ellis, and D. Zeppenfeld, pp. 47–77, (Fermilab, Batavia, 2000), FERMILAB-PUB-00-297.

[20] $\mathcal{R}$ is defined as $\mathcal{R} = \sqrt{(\Delta\eta)^2 + (\Delta\phi)^2}$. The rapidity $y$ and pseudorapidity $\eta$ are defined as functions of the polar angle $\theta$ and parameter $\beta$ as $y(\theta, \beta) \equiv \frac{1}{2} \ln [(1 + \beta \cos\theta)/(1 - \beta \cos\theta)]$ and $\eta(\theta) \equiv y(\theta, 1)$, where $\beta$ is the ratio of a particle's momentum to its energy. We distinguish detector $\eta$ ($\eta_{det}$) and physics $\eta$, where the former is defined with respect to the center of the detector and the latter with respect to the $p\bar{p}$ interaction vertex. $\phi$ is the azimuthal angle around the beamline.

[21] A. Bhatti *et al.*, Nucl. Instrum. Methods A **566**, 375 (2006).

[22] V. M. Abazov *et al.* (D0 Collaboration), Nucl. Instrum. Methods Phys. Res. A **620**, 490 (2010).

[23] D. Acosta et al. (CDF Collaboration), Phys. Rev. D **71**, 052003 (2005).

[24] F. Deliot, D. Glenzinski, Rev. Mod. Phys. **84**, 211 (2012).

[25] M. L. Mangano, M. Moretti, F. Piccinini, R. Pittau, and A. D. Polosa, J. High Energy Phys. **07**, 001 (2003).

[26] T. Sjöstrand, L. Lönnblad, and S. Mrenna, hep-ph/0308153 (2003); we used version 6.2 (CDF) and 6.3 (D0).

[27] M. L. Mangano, M. Moretti, F. Piccinini, and M. Treccani, J. High Energy Phys. **01**, 013 (2007).

[28] R. Brun and F. Carminati, CERN Program Library Long Writeup W5013, 1993 (unpublished).

[29] E. Gerchtein and M. Paulini, arXiv:physics/0306031 (2003).

[30] S. Agostinelli et al., Nucl. Instrum. Methods A506, 250 (2003).

[31] A. Varganov *et al.*, CDF conference note 10878.

[32] T. Aaltonen *et al.* (CDF Collaboration), Phys. Rev. D 81, 052011 (2010).

[33] T. Aaltonen *et al.* (CDF Collaboration), Phys. Rev. Lett. **105**, 012001 (2010).

[34] V. Abasov *et al* (D0 collaboration), Phys. Rev. D **84**, 012008 (2011).

[35] V. Abasov *et al* (D0 collaboration), Phys. Lett. B **704**, 403 (2011).

[36] J. Pumplin *et al.*, (CTEQ Collaboration), J. High Energy Phys. **07**, 012 (2002).

[37] H. L. Lai *et al.*, Eur. Phys. J. C **12**, 375 (2000).

[38] J. M. Campbell and R. K. Ellis, Nucl. Phys. Proc. Suppl. **205-206**, 10 (2010).

[39] E. Boos *et al.*, (CompHEP Collaboration), Nucl. Instrum. Methods Phys. Res. A **534** (2004) 250.

[40] J. Alwall *et al.*, J. High Energy Phys. **28**, 709 (2007).

[41] N. Kidonakis, Phys. Rev. D **74**, 114012 (2006).

[42] B. W. Harris, E. Laenen, L. Phaf, Z. Sullivan, and S. Weinzierl, Phys. Rev. D **66**, 054024 (2002).

[43] U. Baur and E. L. Berger, Phys. Rev. D **41**, 1476 (1990).

[44] A. Abulencia *et al.* (CDF Collaboration), J. Phys. G G **34**, 2457 (2007).

[45] L. Lyons, D. Gibaut and P. Clifford, Nucl. Instrum. Methods in Phys. Res. Sect. A **270**, 110.

[46] L. Lyons, A. Martin and D. Saxon, Phys. Rev. D **41**, 3 (1990).

[47] A. Valassi, Nucl. Instrum. Methods in Phys. Res. Sect. A **500**, 391 (2003).

[48] G. Corcella *et al.*, J. High Energy Phys. **01**, 010 (2001).

[49] S. Frixione, B.R. Webber, J. High Energy Phys. **06**, 029 (2002).

[50] D. Stump *et al.*, J. High Energy Phys. **10**, 046 (2003).

[51] A. Abulencia *et al.* (CDF Collaboration), Phys. Rev. D **73**, 032003 (2006).

[52] K. Nakamura *et al* (Particle Data Group), J. Phys. G **37**, 075021 (2010).

[53] A. Abulencia *et al.* (CDF Collaboration), J. Phys. G G **34** (2007) 2457.

[54] S. Klimenko, J. Konigsberg and T. M. Liss, FERMILAB-FN-0741.

[55] S. Jindariani *et al.*, CDF note 7446; T. Andeen *et al.*, Report No. FERMILAB-TM-2365, 2007.